Published in final edited form as:
Biomaterials. 2010 September ; 31(26): 6772–6781. doi:10.1016/j.biomaterials.2010.05.047.

Hyaluronic Acid Hydrogels with Controlled Degradation Properties for Oriented Bone Regeneration

J Patterson[a,d], **R Siew**[a], **SW Herring**[b], **ASP Lin**[c], **R Guldberg**[c], and **PS Stayton**[a]

[a]Department of Bioengineering, University of Washington, Seattle, WA, 98195, USA

[b]Departments of Orthodontics and Oral Biology, University of Washington, Seattle, WA, 98195, USA

[c]Department of Bioengineering, Georgia Institute of Technology, Atlanta, GA, 30332, USA

Abstract

Non-healing fractures can result from trauma, disease, or age-related bone loss. While many treatments focus on restoring bone volume, few try to recapitulate bone organization. However, the native architecture of bone is optimized to provide its necessary mechanical properties. Hyaluronic acid (HA) hydrogel scaffold systems with tunable degradation properties were developed for the controlled delivery of osteoinductive and angiogenic growth factors, thus affecting the quantity and quality of regenerated tissue. HA hydrogels were designed to degrade at fast, intermediate, and slow rates due to hydrolysis and further provided controlled release of cationic proteins due to electrostatic interactions. Scaffolds delivering bone morphogenetic protein-2 (BMP-2) were evaluated in a rat calvarial bone critical size defect model. BMP-2 delivery from the HA hydrogels had a clear osteoinductive effect *in vivo* and, for all hydrogel types, BMP-2 delivery resulted in significant mineralization compared to control hydrogels. The temporal progression of this effect could be modulated by altering the degradation rate of the scaffold. All three degradation rates tested resulted in similar amounts of mineral formation at the latest (six week) time point examined. Interestingly, however, the fastest and slowest degrading scaffolds seemed to result in more organized bone than the intermediate degrading scaffold, which was designed to degrade in 6–8 weeks to match the healing time. Additionally, healing could be enhanced by co-delivery of vascular endothelial growth factor along with BMP-2.

1. Introduction

Bone regeneration naturally occurs through one or more of three well-established mechanisms of action: osteoinduction, osteoconduction, and osteogenesis [1,2], which can be exploited for the design of regenerative matrices. For example, osteoconductive materials can be used as a scaffold to support and encourage cellular ingrowth while osteoinductive molecules can be incorporated and/or released to stimulate bone formation. This approach was utilized to design scaffolds to test the hypothesis that the rate of scaffold degradation can modulate the amount and organization of bone formation in a critically sized defect model. A calvarial defect model was chosen because it is a standard model that can be

[d]Corresponding author jp98@u.washington.edu.

compared with other studies and because craniofacial defects represent a very large proportion of clinical situations needing bone regeneration. Unlike limbs, where traumatic injuries and cancer surgeries remove large portions of bone, there are no available functional prostheses.

Hyaluronic acid (HA), [α-1,4-D-glucuronic acid-β-1,3-*N*-acetyl-D-glucosamine]$_n$, was chosen as the base matrix because of its demonstrated potential as a scaffold material. HA is a naturally occurring, hydrophilic, nonimmunogenic glycosaminoglycan. HA accumulates during morphogenesis [3], may contribute to fetal scarless healing [4], and plays a role in wound healing [5]. Of relevance to bone, HA has been found in high concentrations in the early fracture callus [6], in lacunae surrounding hypertrophic chondrocytes in the growth plate [7], and in the cytoplasm of osteoprogenitor cells [7]. HA has been shown to support bone growth in combination with other osteoconductive molecules, such as collagen [8], and is able to increase some markers of differentiation in cultured osteoblasts with dose and size dependent effects [9]. HA can be modified and crosslinked into a hydrogel to form a more stable scaffold by a number of strategies, including diepoxy, carbodiimide-mediated, aldehyde, divinyl sulfone, and photo-crosslinking (reviewed in [10]) as well as reversible disulfide crosslinking [11]. In the current study, a photo-crosslinking method was utilized, based on published reports [12,13], where reactive methacrylate groups *in vitro* are attached to the HA backbone and free radical polymerization is induced by ultraviolet (UV) irradiation. Hydrogels produced using a similar chemistry were found to be cytocompatible when exposed to human aortic endothelial cells (HAEC) *in vitro* as well as to support endothelial cell migration *in vivo* [13]. Further, HA hydrogels were able to maintain >95% viability of encapsulated fibroblasts and to support neocartilage formation *in vivo* when used to implant encapsulated chondrocytes [14].

Optimally, scaffolds for regenerative medicine applications should degrade over the course of tissue regeneration to allow complete repair by host tissue. In the case of HA, while the backbone itself should be degraded by hyaluronidase *in vivo*, additional degradable sites can be engineered into the hydrogel network during crosslinking. For example, crosslinking HA with a diepoxy compound results in an ether linkage that is slowly degradable under physiologic conditions [15]. Characterization of the degradation of photo-crosslinked HA hydrogels has generally focused on the ability of hyaluronidase to degrade the chemically modified and crosslinked forms of HA. However, it is likely that these hydrogels would see much lower levels of hyaluronidase activity *in vivo* as serum levels are low [4,16] and an acidic pH (presumably within a cell or lysosome) is needed for optimum enzyme activity [17]. Therefore, this study has also examined the ability of HA hydrogels to degrade via hydrolysis, and the chemistry used to prepare the HA hydrogels was manipulated to obtain three distinct degradation rates. The final parameter in selecting HA as a matrix material is its ability to provide controlled release of proteins, which can be achieved by diffusion dependent on gel mesh size and electrostatic interactions between the negatively charged HA and positively charged proteins. Diffusion limited protein release has been shown for HA hydrogels with further control provided by the incorporation of degradable microspheres [18]. Electrostatic interactions of HA hydrogels with cationic molecules have been shown for the model drug chlorpromazine HCl [19]. In the current study, it is expected that the HA hydrogels would provide controlled release of cationic osteoinductive and angiogenic proteins. A well-established osteoinductive molecule [20,21], bone morphogenetic protein-2 (BMP-2) is suited for delivery from HA hydrogels due to its basic isoelectric point, both measured (pI > 8.5 [22]) and calculated (pI = 9.16, EMBL WWW Gateway to Isoelectric Point Service, sequence from [21]). Naturally, BMPs are presented in the context of the extracellular matrix (ECM) and can bind to heparin sulfate, heparin, and type IV collagen [23]. The efficacy of BMP-2 can be enhanced by extended localized release, as has been shown in a comparison of immediate *versus* sustained release formulations of microspheres

[24]. More sophisticated scaffolds have been developed to release matrix-bound BMP-2 upon cleavage of a fusion protein by cell-surface associated proteases and to induce bone formation *in vivo* [25]. BMP-2 has previously been delivered from a crosslinked gelatin hydrogel system [26], and it has successfully been used with non-crosslinked HA carriers in bone defect models [27,28]. The present study extends this line of work and utilizes photo-crosslinked HA hydrogels to deliver BMP-2. The ability to control the degradation rate of the crosslinked scaffold and thus the persistence of both BMP-2 and HA in the defect site allows interesting questions to be asked about the temporal progression of bone regeneration and the suitability of this scaffold material delivery system. In addition to standard measures of bone formation, i.e., measuring the extent of mineralization, the effect of the different treatments on the organization of collagen in the regenerating bone was examined.

Vascular endothelial growth factor (VEGF) is one of the most potent angiogenic molecules, and it is capable of inducing endothelial cell migration *in vitro* [29] and angiogenesis *in vivo* [30]. VEGF is a 45 kDa homodimeric glycosylated protein with four alternatively spliced variants that have increasing affinity for heparin: $VEGF_{121}$, $VEGF_{165}$, $VEGF_{189}$, and $VEGF_{206}$ [29]. VEGF can be released from the ECM by plasmin cleavage as well as through degradation of the heparin matrix [31,32]. Therefore, retention of VEGF within HA hydrogel scaffolds may mimic natural tissue inductive processes. The isoelectric point of $VEGF_{165}$ has been measured at 8–8.5 [30] and was calculated to be 7.29 (EMBL WWW Gateway to Isoelectric Point Service, sequence from [33]) so it should also bind to HA. Controlled, localized delivery of VEGF is important for optimal effects, as has been shown with calcium alginate microsphere [34] and enzymatically cleavable [35] delivery systems.

Interestingly, VEGF appears to be able to directly affect osteoblasts and osteoclasts *in vitro*. VEGF was able to induce osteoblast differentiation in cultured progenitors [36,37] and can increase mineralization in calvarial explants [38]. Despite these observations and further links between angiogenesis and bone growth during endochondral ossification [39], fracture repair [40], and distraction osteogenesis [41,42], few groups have attempted to deliver angiogenic factors as a treatment to regenerate bone. Street *et al.* showed significant increases in calcified callus with sustained release of VEGF in both a murine femoral fracture model and a rabbit radius segmental gap model [43]. Murphy *et al.* developed mineralized, porous, poly(lactide-co-glycolide) (PLGA) scaffolds for the controlled release of VEGF [44], which significantly enhanced vascularization and mineralization in a rat calvarial critical size defect model, although there was no significant difference in osteoid compared to the mineralized scaffold without VEGF [45]. Endogenous VEGF has been shown to contribute to BMP-2 mediated bone formation, although VEGF delivery alone was insufficient to induce bone formation in the calvarial defect model [46]. Further, exogenous VEGF administration enhanced BMP-2 mediated bone formation, particularly by increasing angiogenesis and cartilage resorption [46]. Therefore, the effects of co-delivery of BMP-2 and VEGF were also explored in the present study.

2. Materials and Methods

2.1. Glycidyl Methacrylate Modified HA (HA-GMA) Preparation Methods, after [47,48]

HA (220kDa, Lifecore) at 14.3 mg/mL (pH 9) was reacted with a 29-fold molar excess of glycidyl methacrylate (GMA) at room temperature for 7 days. The reaction was stopped by adjusting the pH to 7, and the HA-GMA (220kDa) was purified by 2X precipitation in tetrahydrofuran (THF). HA (110kDa, Lifecore) was first converted to the tetrabutyl ammonium (TBA) salt form and dissolved at 20 mg/mL in dimethyl sulfoxide (DMSO). It was reacted with a 2-fold molar excess of GMA in the presence of a 5-fold molar excess of 4-(dimethylamino)pyridine (DMAP) at 30°C for 16 hours. The reaction was stopped by

adding 10% v/v 2.5M NaCl, and the HA-GMA (110kDa) was purified by 2X precipitation in acetone followed by dialysis.

2.2. HA-GMA Characterization

For gel permeation chromatography (GPC), HA-GMA was dissolved at 3–6 mg/mL in phosphate buffer (PB), pH 8.0, and was run on a GPCMax (Viscotek) using poly(ethylene oxide) (PEO) standards. For ^{1}H- and ^{13}C-NMR, HA-GMA was dissolved at a minimum concentration of 10 mg/mL in deuterium oxide (D_2O, Cambridge Isotope Laboratories). Spectra were obtained on a Bruker Avance DRX series instrument at a frequency of 499.85 MHz or AV series instrument at a frequency of 500.046 MHz. The degree of substitution (number of methacrylate groups per 100 disaccharide units) was calculated from the ^{1}H-NMR spectra by taking ratios of the acrylate peaks at ~5.6 and ~6.1 ppm, which arise from the methacrylate group only, and the methyl peak at 1.9 ppm, which includes protons from the methacrylate group and backbone methyl group. Extent of crosslinking, which should decrease the acrylate peaks, was determined by degrading crosslinked HA-GMA hydrogels at pH 2 and 100°C for 4 hours prior to analysis by ^{1}H-NMR.

2.3. HA Hydrogel Formation and Characterization

HA-GMA was dissolved in DI water at 20 mg/mL (220kDa) or at 30 mg/mL (110kDa). In some cases, mixtures of these starting solutions, increased HA-GMA concentrations, or 1-vinyl-2-pyrrolidinone (NVP) as a co-monomer were used. The HA-GMA solution was mixed with a photo-initiator in a volume ratio of 10:1 (HA-GMA:initiator). The photo-initiator, 2-hydroxy-1-[4-(hydroxyethoxy)phenyl]-2-methyl-1-propanone (Irgacure®2959, Ciba), was dissolved at a concentration of 20 mg/mL in methanol. Crosslinking was initiated by exposure to UV irradiation (365nm) for 20–30 minutes. After formation, the hydrogels were rinsed, lyophilized, and then rehydrated. The swelling ratio, which should indicate the extent of functional crosslinks formed, was taken as the wet weight of the hydrogels after equilibration in excess DI water (W_s)/dry weight of the hydrogel (W_d). The elastic and storage moduli were determined for crosslinked HA-GMA films using an AR2000 rheometer (TA Instruments) with 40mm parallel plate geometry. The HA-GMA was directly crosslinked on the bottom plate, and the top plate was lowered until the normal force measured ~1N. Measurements were taken at 37°C using a stress sweep from 1–1000 Pa at an angular frequency of 6.283 rad/s.

2.4. Characterization of Hydrolytic Degradation

Hydrogels (100μL) were suspended at 37°C in 1mL of buffer [phosphate buffered saline (PBS, pH 7.4), 138mM NaCl in unbuffered DI water (pH ~5.5), or 0.1M carbonate buffer (pH 10.0)]. The buffer was completely removed and replaced at selected time points, and the amount of HA released was quantified by a carbazole assay in a 96-well plate format, after [49].

2.5. In Vitro Protein Release

Lyophilized hydrogels (100μL) were rehydrated with 100μL of 0.01 mg/mL BMP-2 (R&D Systems) or VEGF (Genentech) in 0.1% bovine serum albumin (BSA) in PBS or 0.01% BSA in PBS as a control. After equilibration for 1 hour, the gels were suspended in 1mL of 0.1% BSA in PBS (PBS only for control) and placed at 37°C. The buffer was completely removed and replaced at selected time points. The concentration of BMP-2 or VEGF in the release buffer was measured by ELISA (R&D Systems) whereas BSA was measured by a Bradford assay (Coomassie Plus, Pierce). At the final time point, any remaining hydrogels were degraded with 1mL of 500 U/mL hyaluronidase at 37°C overnight, and the residual protein was measured.

2.6. Rat Calvarial Critical Size Defect Model

Hydrogels (35μL) were aseptically prepared from sterile-filtered solutions and formed into disks using 5mm diameter Teflon molds. Lyophilized hydrogels were rehydrated with 35μL of sterile PBS (control) or sterile PBS with 5μg BMP-2 and/or 25μg VEGF. The surgical protocol was conducted under approval from the University of Washington (UW) Institutional Animal Care and Use Committee. Animals were housed in a specific pathogen free environment with 12-hour light/dark cycles at the UW Department of Comparative Medicine and had *ad libitum* access to food and water. Adult male Sprague Dawley rats (Harlan) were anesthetized using isoflurane (5% induce; 2.5% maintain) and were administered buprenorphine immediately pre-operatively for pain mitigation. The surgical site was shaved and disinfected. A linear incision was made along the midline of the scalp, and the soft tissues and periosteum were reflected. A 5mm diameter circular, full thickness defect was made in the parietal bones, centered over the sagittal suture line, using a Command2 drill system with 1.0mm cross-cut fissure carbide bur (Stryker) while irrigating with saline. The defect site was rinsed extensively with saline, the implant was placed into the defect, and the soft tissues were closed over the defect site using wound clips. Power calculations were performed using the DSTPLAN distribution. Assumptions for the expected means and standard deviations were based on results from a preliminary study comparing a negative control (no implant) with a scaffold loaded with BMP. A minimum sample of 4 was required for 80% power and 5% significance when comparing the positive and negative groups. Therefore, a minimum of 6 rats was used for all treatment groups except those receiving VEGF, which had n=4.

2.7. Tissue Harvest and Analysis

After allowing the defect to heal for 3 or 6 weeks, the animals were sacrificed by carbon dioxide (CO_2) asphyxiation. The parietal bones were harvested and fixed in 10% neutral buffered formalin (Fisher) for 24 hours at room temperature. The bone pieces were rinsed and stored in 70% ethanol at 4°C. Microcomputed tomography (microCT) analysis was performed using a vivaCT 40 (Scanco) with E = 55kVp, I = 109μA, and voxel size = 21μm. A 5mm diameter × 1mm tall region centered within the defect was analyzed for each sample using segmentation parameters of sigma = 1.2, support = 2, and threshold = 143. The bone pieces were then decalcified in 10% EDTA, pH 7, for 10–14 days at room temperature. Paraffin-embedded sections (5μm) were stained with hematoxylin and eosin (H&E) or Masson's trichrome and viewed using brightfield microscopy (E800 microscope, Nikon). To view the collagen orientation, tissue sections were stained with 0.1% sirius red (Direct Red 80) in a saturated aqueous solution of picric acid for one hour, rinsed in 0.5% acetic acid, and viewed under polarized light. The sections were oriented so that the lamellar collagen in the native bone at the edges of the defect was approximately 45°to the incident light. This should result in maximal birefringence for newly formed bone that is oriented in the same direction as the native bone. The amount of organized bone was quantified by thresholding the images using the green color of the native lamellar bone.

2.8. Statistical Analysis

Data were analyzed using the GraphPad Prism software package. One, two, or three factor ANOVAs with appropriate post-tests were performed as indicated in the results. Differences were considered statistically significant when the p-value was less than 0.05.

3. Results

3.1. HA Modification, Characterization, and Hydrogel Formation

Both HA-GMA (220kDa) and HA-GMA (110kDa) had a degree of substitution of approximately 17, and no degradation of the HA occurred. As indicated by the presence of four additional peaks in the ^{13}C-NMR spectra of HA-GMA (110kDa) (Figure 1C, arrows) compared to unmodified HA (Figure 1A), HA-GMA (110kDa) appeared to have an addition of just the methacrylate group from GMA to the HA backbone. HA-GMA (220kDa) also had four peaks from the methacrylate group (Figure 1B, arrows). However, further additional peaks around δ = 68–74 ppm (Figure 1B, box) indicated the presence of the glyceryl spacer in addition to the methacrylate group from GMA. The crosslinking conditions resulted in the conversion of approximately 90% of the reactive vinyl groups, indicating that the gels were well-crosslinked. Hydrogels prepared from HA-GMA (220kDa) had a swelling ratio of 88, which corresponds to a water content of 99%. The swelling ratio decreased with increasing HA-GMA degree of substitution, indicating a higher crosslink density (data not shown).

3.2. HA-GMA Hydrogel Degradation and Protein Release

Whereas the HA-GMA (220kDa) hydrogels were stable in citrate buffer (pH 5.3) and in DI water (pH ~5.5), degradation of the hydrogels via hydrolysis was rapid at physiologically relevant conditions (Figure 2). Hydrolytic degradation was base catalyzed (pH 10.0 > pH 7.4 > pH 5.5; data not shown). Further confirmation that hydrolysis was affecting the ester bonds in the crosslinks and not degrading the HA backbone was confirmed by GPC analysis of unmodified HA incubated in similar buffers. Increasing the HA-GMA concentration or using a co-monomer, such as NVP, to increase interchain crosslinks resulted in slowed degradation of the hydrogels (data not shown). Interestingly, hydrogels prepared from HA-GMAs made using other methods but with similar degrees of substitution had different hydrolytic degradation behaviors. HA-GMA (110kDa) hydrogels were stable for several months in PBS at 37°C (Figure 2). Therefore, HA-GMA hydrogels with three different hydrolytic degradation rates were targeted. HA-GMA (220kDa) at 20 mg/mL resulted in hydrogels that degraded in one week in PBS, pH 7.4, at 37°C and will be referred to as “fast degrading” hydrogels. HA-GMA (110kDa) at 30 mg/mL resulted in hydrogels that did not degrade even after several months and will be referred to as “slow degrading” hydrogels. Mixtures of the starting solutions (20 mg/mL 220kDa and 30 mg/mL 110kDa) were made at various ratios (25:75, 50:50, 75:25), and the hydrogels formed had degradation rates that fell between the fast and slow degrading hydrogels. The 50:50 mixture resulted in a hydrogel that degraded in 6–8 weeks and was selected as an “intermediate degrading” hydrogel formulation (Figure 2). The rheological properties of these formulations were also examined, and all three had similar moduli (1–2Pa for G’ and 3–5Pa for G”). To confirm that the chemical modifications to the HA would not prevent degradation by hyaluronidase, HA-GMA hydrogels were successfully degraded in various concentrations of hyaluronidase (data not shown).

BSA (pI ~5.8) was used as a model protein to show diffusion-limited release. VEGF and BMP-2 are both cationic proteins, and their release was slowed compared to BSA for all hydrogel types (Figure 3). Further, altering the degradation rate of the hydrogels affected the release rates of BMP-2 and VEGF. The fast degrading hydrogels released all of their BMP-2 rapidly along with hydrogel degradation. The slow degrading hydrogels had a high burst release of BMP-2, which was followed by release at nanogram levels per week. When the still intact slow degrading hydrogels were degraded at 8 weeks, a reservoir of approximately 20% BMP-2 was found to be retained in the HA hydrogel. Similar to their degradation rates, the intermediate degrading hydrogels had intermediate release profiles. Release of BMP-2

was fairly rapid for the first week. It slowed over the next 7 weeks, although still remaining faster than release from the slow degrading hydrogels, and almost 100% was released by the final 8 week time point. Similar behavior was observed for VEGF release from the HA hydrogels with VEGF being released faster than BMP-2 but slower than BSA.

3.3. In Vivo Bone Regeneration with BMP-2

As seen in Figure 4, significant bone formation was induced for all three scaffold types in BMP-2 treated animals compared to controls at both the 3 week and 6 week time points ($p < 0.001$). A three factor ANOVA including interaction terms followed by a Tukey HSD post-test was significant at $p < 0.0001$. The ANOVA indicated that both BMP-2 treatment and time had significant effects, while the mineral volume formed was insensitive to the type of hydrogel. It can be clearly seen that the mineral volume in the BMP-2 treated animals was similar for all three hydrogel types at 6 weeks. Further, the difference in mineralization between the control and BMP-2 treated defects was larger at 6 weeks compared to 3 weeks (interaction term of BMP-2 treatment and time at $p < 0.0001$), suggesting a sustained effect of BMP-2 delivery.

Examination of histological sections stained with Masson's trichrome at the early time point showed minimal new bone formation for all three control hydrogel groups (Figure 5). The fast and intermediate degrading hydrogels with BMP-2 had new bone completely bridging the defect. The slow degrading hydrogels with BMP-2 had impeded new bone formation as the hydrogel, which appears as a clear region in the histological sections, filled much of the defect space keeping new bone formation limited to the periphery of the implant. By 6 weeks (Figure 6), the control groups continued to have minimal new bone growth into the defect site although some remodeling was seen at the native bone edges. The fast and intermediate degrading hydrogels with BMP-2 appeared qualitatively similar to the 3 week samples. For the slow degrading hydrogels with BMP-2, additional new bone was formed compared to the 3 week time point. A clear region resulting from the residual hydrogel was still present in the histological sections; however, it was smaller and the defect was filled with new bone between the native bone edges and the residual scaffold. It is interesting to note that the slow degrading hydrogels with BMP-2 resulted in similar levels of mineralization as the fast and intermediate degrading hydrogels with BMP-2 at the 6 week time point since the defect is not completely healed by this point and there would be additional space for bone to grow as the hydrogel scaffold continues to degrade. Therefore, it is likely that this new bone is less porous.

3.4. Collagen Orientation

While BMP-2 delivery from the HA hydrogel scaffolds can clearly induce mineralized bone tissue formation, an interesting additional question is whether the degradation rate of the scaffold can affect the organization of the collagen matrix in the regenerating bone. Polarized light microscopy allows one to examine the orientation of collagen by utilizing its natural birefringence, which is enhanced by picrosirius red. In picrosirius red stained sections (Figure 7A–E), well-ordered collagen in the native bone and in regions of the newly formed bone appeared green while disordered collagen appeared red. Interestingly, while the slow degrading hydrogels with BMP-2 had the least area of new bone tissue formation because the residual scaffold took up a large region of the defect, the new bone seemed well organized. Organized bone was also seen in the fast degrading hydrogels with BMP-2 while less organized bone was seen in the intermediate degrading samples. Quantitatively, both fast and slow degrading samples had more organized bone than the intermediate degrading samples (Figure 7F). A one-way ANOVA indicated a significant effect of scaffold type ($p < 0.05$). Interestingly, the % threshold for the fast and slow degrading samples became

approximately the same when the area of the residual scaffold was subtracted from measurements of the slow degrading samples.

3.5. In Vivo Bone Regeneration with VEGF

Neither 5μg nor 25μg VEGF delivered from the fast degrading hydrogels resulted in significant mineralization after 6 weeks of healing. Co-delivery of 25μg VEGF and 5μg BMP-2 from the fast degrading hydrogels was compared to delivery of VEGF or BMP-2 alone (Figure 8). A two factor ANOVA followed by a Bonferroni post-test indicated significant effects of BMP-2 ($p \mu 0.0001$) and VEGF ($p < 0.05$). While 25μg VEGF did not increase mineralization compared to unloaded hydrogel controls, delivery of 25μg VEGF in combination with 5μg BMP-2 significantly increased the mineral formation compared to BMP-2 delivery alone ($p < 0.05$). Further, delivery of VEGF in addition to BMP-2 did not affect collagen orientation, with the oriented collagen area remaining at the same (highest) level as delivery of BMP-2 from the same scaffold type (Figure 7).

4. Discussion

Hydrogels prepared from HA-GMAs with similar degrees of substitution had similar swelling ratios but exhibited different hydrolytic degradation behavior. The main difference between the two types of hydrogels was that HA-GMA (220kDa) was prepared under basic aqueous conditions while HA-GMA (110kDa) was prepared from the TBA salt form in DMSO. Tomihata and Ikada suggest that a water content below 90% is needed to slow hydrolytic degradation of HA hydrogels [15]; however, all groups of the HA-GMA hydrogels had a water content greater than 95%. The stability of hydrogels formed from HA-GMA (110kDa) suggests that water content alone might not affect the likelihood of degradation but that there might be some chemical difference between the HA-GMAs. The ester bonds in the crosslinked HA-GMA hydrogels may degrade through a hydrolytic mechanism as has previously been shown for the ether linkages formed by crosslinking HA with a diepoxy compound [15] and for the ester bonds of crosslinked glycidyl methacrylate derivatized dextran [50]. Different esters can be formed from the addition of GMA to HA, if there is transesterification (transfer of only the methacrylate group) or if there is an epoxide ring opening (resulting in the presence of an additional glyceryl spacer). Additionally, the pH of the reaction mixture may affect the selectivity between reaction with the hydroxyl and carboxyl groups on the HA backbone. Detailed studies of diepoxy cross-linking chemistry have shown that at low pH, diepoxy compounds form ester linkages between carboxyl groups, whereas at high pH, they form ether linkages between hydroxyl groups [51]. It seems to be a reasonable hypothesis, then, that a chemical difference could be responsible for the difference in hydrolytic degradation behavior that was observed. Differences in the ^{13}C-NMR spectra suggest that the slow degrading hydrogels may have the methacrylated product formed via transesterification while the fast degrading hydrogels may have an additional glyceryl spacer.

The ability of the scaffolds to degrade with time motivated the selection of HA because degradation affects both protein release and tissue infiltration. The HA-GMA hydrogels should degrade *in vivo* through two mechanisms: hydrolysis as discussed and enzymatic degradation of the HA backbone. However, the wide variation in hyaluronidase levels in various tissues and its dependence on the specific cells present make it difficult to select a relevant concentration for *in vitro* testing. This variability in hyaluronidase concentration could further result in differences in HA persistence at different implant sites. Therefore, the ability to control HA hydrogel degradation through hydrolytic mechanisms may be more likely to result in a hydrogel that will degrade in a controlled fashion *in vivo*These results also demonstrate that while electrostatic interactions may slow diffusion of cationic proteins such as BMP-2 and VEGF from the intact scaffolds, degradation of the scaffolds *in vivo*

through hydrolysis or hyaluronidase activity should release BMP-2 or VEGF from the scaffolds.

In this study, HA-GMA hydrogels were shown to be able to support bone growth *in vivo* when used with appropriate osteoinductive molecules. By utilizing mixtures of two different forms of HA-GMA, hydrogels with a range of degradation rates were prepared. These hydrogels should present a similar chemical and mechanical environment while allowing the persistence of HA and BMP-2 within the defect site to be varied. Altering the degradation rate of the scaffold could modulate the temporal progression of bone formation and remodeling. Interestingly, all three degradation rates tested resulted in similar amounts of mineral formation at the latest time point examined. However, the fastest and slowest degrading scaffolds seemed to result in more organized collagen deposition than the intermediate degrading scaffold, which was designed to degrade in 6–8 weeks to approximate the end point of the study. It is possible that a degradation time of 6–8 weeks is not matched to an optimal healing time. However, the improved collagen orientation seen with the fast and slow degrading hydrogels suggests some interesting alternatives. The fast degrading hydrogels with BMP-2 may be able to quickly induce enough bone formation that the collagen matrix then had time to remodel during the six weeks of healing. In contrast, the slow degrading hydrogels with BMP-2 may retard bone formation enough so that the collagen is deposited in a more organized fashion from the beginning. Because there is only a small space available, the deposited collagen has to align itself. The results of this study suggest that analysis of bone regeneration in this model and with these materials should be taken out to later time points. It is likely that increased mineralization would be seen at later time points, particularly for the slow degrading hydrogels, as a large area remains to be filled with bone even at week 6. VEGF did not have an osteoinductive effect *in vivo* when delivered alone. Use of radiographs to measure mineralization indicated that VEGF might have had a potential dose effect; however, this was not confirmed by the more sensitive technique of microCT. Qualitative examination of the harvested tissues using histology generally indicated a greater tissue volume filling the defect area for samples treated with VEGF compared to controls, which could account for the increased radioopacity. As bone has been shown to regenerate in the calvaria through a mechanism similar to intramembranous ossification [52] and VEGF may not have strong osteogenic activity there [46], unsuccessful treatments may have different effects in other anatomical locations. Further, while angiogenesis has synergistic effects on bone growth, VEGF delivery alone may interfere with bone growth as VEGF has been shown to stimulate osteoclast differentiation [53] and monocyte chemotaxis [54]. Importantly, however, co-delivery of VEGF and BMP-2 showed an increase in mineral formation compared to delivery of BMP-2 alone. The angiogenic factor, while ineffective at stimulating bone growth on its own, may be acting to increase mineral formation by increasing blood vessel formation and thus nutrient delivery to the regenerating tissue. The interrelations of VEGF with bone cells and BMPs are very complex, and understanding the mechanisms of the effect of co-delivery will be the subject of future work. For example, further examination of the effects of VEGF on angiogenesis as well as on the amount of cellular infiltration and/or ECM production is warranted.

5. Conclusions

Overall, these results support the hypothesis that the rate of scaffold degradation can modulate the formation of mature bone. The scaffold degradation rate had an effect on bone healing, specifically affecting the organization of the collagen matrix. Additionally, the co-delivery of an angiogenic molecule in conjunction with an osteoinductive molecule increased the amount of mineralized tissue formed. These materials have potential for clinical application to bone defects, particularly in the craniofacial skeleton. While the

mechanical properties of the hydrogels may be too low to support a mechanically loaded environment themselves, HA-GMA hydrogels could be utilized as a bioactive component in a composite scaffold or with a fixation device to provide the necessary mechanical support.

Acknowledgments

This work was supported in part by the National Institutes of Health and the National Science Foundation (NSF Graduate Fellowship to J. Patterson, University of Washington Engineered Biomaterials (UWEB) Center NSF grants # EEC-9872882 and #EEC-9529161, Bioengineered Allogeneic Tissue (BEAT) partnership NIH grant #5 R24 HL64387). Microscopy was performed in the UWEB Microscopy and Image Analysis Resource, directed by Dr. Kip Hauch.

References

1. Athanasiou KA, Zhu C, Lanctot DR, Agrawal CM, Wang X. Fundamentals of biomechanics in tissue engineering of bone. Tissue Eng 2000;6(4):361–381. [PubMed: 10992433]
2. Lane JM, Sandhu HS. Current approaches to experimental bone grafting. Orthop Clin North Am 1987;18(2):213–225. [PubMed: 3550572]
3. Toole BP. Hyaluronan in morphogenesis. J Intern Med 1997;242(1):35–40. [PubMed: 9260564]
4. West DC, Shaw DM, Lorenz P, Adzick NS, Longaker MT. Fibrotic healing of adult and late gestation fetal wounds correlates with increased hyaluronidase activity and removal of hyaluronan. Int J Biochem Cell Biol 1997;29(1):201–210. [PubMed: 9076955]
5. Chen WY, Abatangelo G. Functions of hyaluronan in wound repair. Wound Repair Regen 1999;7(2):79–89. [PubMed: 10231509]
6. Hollinger J. Factors for osseous repair and delivery. Part I. J Craniofac Surg 1993;4(2):102–108. [PubMed: 8324082]
7. Pavasant P, Shizari TM, Underhill CB. Distribution of hyaluronan in the epiphysial growth plate: turnover by CD44-expressing osteoprogenitor cells. J Cell Sci 1994;107(Pt 10):2669–2677. [PubMed: 7533172]
8. Liu LS, Thompson AY, Heidaran MA, Poser JW, Spiro RC. An osteoconductive collagen/hyaluronate matrix for bone regeneration. Biomaterials 1999;20(12):1097–1108. [PubMed: 10382825]
9. Huang L, Cheng YY, Koo PL, Lee KM, Qin L, Cheng JCY, et al. The effect of hyaluronan on osteoblast proliferation and differentiation in rat calvarial-derived cell cultures. J Biomed Mater Res A 2003;66(4):880–884. [PubMed: 12926041]
10. Leach JB, Bivens KA, Collins CN, Schmidt CE. Development of photocrosslinkable hyaluronic acid-polyethylene glycol-peptide composite hydrogels for soft tissue engineering. J Biomed Mater Res A 2004;70(1):74–82. [PubMed: 15174111]
11. Shu XZ, Liu Y, Luo Y, Roberts MC, Prestwich GD. Disulfide cross-linked hyaluronan hydrogels. Biomacromolecules 2002;3(6):1304–1311. [PubMed: 12425669]
12. Trudel J, Massia SP. Assessment of the cytotoxicity of photocrosslinked dextran and hyaluronan-based hydrogels to vascular smooth muscle cells. Biomaterials 2002;23(16):3299–3307. [PubMed: 12099272]
13. Leach J, Bivens K, Patrick C, Schmidt C. Photocrosslinked hyaluronic acid hydrogels: Natural, biodegradable tissue engineering scaffolds. Biotechnol Bioeng 2003;82(5):578–589. [PubMed: 12652481]
14. Burdick JA, Chung C, Jia X, Randolph MA, Langer R. Controlled degradation and mechanical behavior of photopolymerized hyaluronic acid networks. Biomacromolecules 2005;6(1):386–391. [PubMed: 15638543]
15. Tomihata K, Ikada Y. Preparation of cross-linked hyaluronic acid films of low water content. Biomaterials 1997;18(3):189–195. [PubMed: 9031718]
16. Frost GI, Stern R. A microtiter-based assay for hyaluronidase activity not requiring specialized reagents. Anal Biochem 1997;251(2):263–269. [PubMed: 9299025]

17. McGuire PG, Castellot JJ, Orkin RW. Size-dependent hyaluronate degradation by cultured cells. J Cell Physiol 1987;133(2):267–276. [PubMed: 3680390]
18. Leach JB, Schmidt CE. Characterization of protein release from photocrosslinkable hyaluronic acid-polyethylene glycol hydrogel tissue engineering scaffolds. Biomaterials 2005;26(2):125–135. [PubMed: 15207459]
19. Inukai M, Jin Y, Yomota C, Yonese M. Preparation and characterization of hyaluronate-hydroxyethyl acrylate blend hydrogel for controlled release device. Chem Pharm Bull (Tokyo) 2000;48(6):850–854. [PubMed: 10866147]
20. Urist MR. Bone: formation by autoinduction. Science 1965;150(698):893–899. [PubMed: 5319761]
21. Wozney JM, Rosen V, Celeste AJ, Mitsock LM, Whitters MJ, Kriz RW, et al. Novel regulators of bone formation: molecular clones and activities. Science 1988;242(4885):1528–1534. [PubMed: 3201241]
22. Wozney JM. Bone morphogenetic proteins. Prog Growth Factor Res 1989;1(4):267–280. [PubMed: 2491264]
23. Paralkar VM, Nandedkar AK, Pointer RH, Kleinman HK, Reddi AH. Interaction of osteogenin, a heparin binding bone morphogenetic protein, with type IV collagen. J Biol Chem 1990;265(28): 17281–17284. [PubMed: 2211625]
24. Woo BH, Fink BF, Page R, Schrier JA, Jo YW, Jiang G, et al. Enhancement of bone growth by sustained delivery of recombinant human bone morphogenetic protein-2 in a polymeric matrix. Pharm Res 2001;18(12):1747–1753. [PubMed: 11785696]
25. Schmoekel HG, Weber FE, Schense JC, Grätz KW, Schawalder P, Hubbell JA. Bone repair with a form of BMP-2 engineered for incorporation into fibrin cell ingrowth matrices. Biotechnol Bioeng 2005;89(3):253–262. [PubMed: 15619323]
26. Yamamoto M, Kato K, Ikada Y. Effect of the structure of bone morphogenetic protein carriers on ectopic bone regeneration. Tissue Eng 1996;2(4):315–326. [PubMed: 19877963]
27. Eckardt H, Christensen KS, Lind M, Hansen ES, Hall DWR, Hvid I. Recombinant human bone morphogenetic protein 2 enhances bone healing in an experimental model of fractures at risk of non-union. Injury 2005;36(4):489–494. [PubMed: 15755429]
28. Arosarena OA, Collins WL. Bone regeneration in the rat mandible with bone morphogenetic protein-2: a comparison of two carriers. Otolaryngol Head Neck Surg 2005;132(4):592–597. [PubMed: 15806052]
29. Leung DW, Cachianes G, Kuang WJ, Goeddel DV, Ferrara N. Vascular endothelial growth factor is a secreted angiogenic mitogen. Science 1989;246(4935):1306–1309. [PubMed: 2479986]
30. Ferrara N, Leung DW, Cachianes G, Winer J, Henzel WJ. Purification and cloning of vascular endothelial growth factor secreted by pituitary folliculostellate cells. Methods Enzymol 1991;198:391–405. [PubMed: 1857232]
31. Houck KA, Leung DW, Rowland AM, Winer J, Ferrara N. Dual regulation of vascular endothelial growth factor bioavailability by genetic and proteolytic mechanisms. J Biol Chem 1992;267(36): 26031–26037. [PubMed: 1464614]
32. Keyt BA, Berleau LT, Nguyen HV, Chen H, Heinsohn H, Vandlen R, et al. The carboxyl-terminal domain (111–165) of vascular endothelial growth factor is critical for its mitogenic potency. J Biol Chem 1996;271(13):7788–7795. [PubMed: 8631822]
33. Weindel K, Marmé D, Weich HA. AIDS-associated Kaposi's sarcoma cells in culture express vascular endothelial growth factor. Biochem Biophys Res Commun 1992;183(3):1167–1174. [PubMed: 1567395]
34. Elçin YM, Dixit V, Gitnick G. Extensive in vivo angiogenesis following controlled release of human vascular endothelial cell growth factor: implications for tissue engineering and wound healing. Artif Organs 2001;25(7):558–565. [PubMed: 11493277]
35. Zisch AH, Lutolf MP, Ehrbar M, Raeber GP, Rizzi SC, Davies N, et al. Cell-demanded release of VEGF from synthetic, biointeractive cell ingrowth matrices for vascularized tissue growth. FASEB J 2003;17(15):2260–2262. [PubMed: 14563693]
36. Midy V, Plouët J. Vasculotropin/vascular endothelial growth factor induces differentiation in cultured osteoblasts. Biochem Biophys Res Commun 1994;199(1):380–386. [PubMed: 8123039]

37. Deckers MM, Karperien M, van der Bent C, Yamashita T, Papapoulos SE, Löwik CW. Expression of vascular endothelial growth factors and their receptors during osteoblast differentiation. Endocrinology 2000;141(5):1667–1674. [PubMed: 10803575]
38. Zelzer E, McLean W, Ng YS, Fukai N, Reginato AM, Lovejoy S, et al. Skeletal defects in VEGF(120/120) mice reveal multiple roles for VEGF in skeletogenesis. Development 2002;129(8):1893–1904. [PubMed: 11934855]
39. Gerber HP, Vu TH, Ryan AM, Kowalski J, Werb Z, Ferrara N. VEGF couples hypertrophic cartilage remodeling, ossification and angiogenesis during endochondral bone formation. Nat Med 1999;5(6):623–628. [PubMed: 10371499]
40. Glowacki J. Angiogenesis in fracture repair. Clin Orthop Relat Res 1998;355(Suppl):S82–S89. [PubMed: 9917629]
41. Li G, Simpson AH, Kenwright J, Triffitt JT. Effect of lengthening rate on angiogenesis during distraction osteogenesis. J Orthop Res 1999;17(3):362–367. [PubMed: 10376724]
42. Choi IH, Chung CY, Cho TJ, Yoo WJ. Angiogenesis and mineralization during distraction osteogenesis. J Korean Med Sci 2002;17(4):435–447. [PubMed: 12172035]
43. Street J, Bao M, deGuzman L, Bunting S, Peale FV, Ferrara N, et al. Vascular endothelial growth factor stimulates bone repair by promoting angiogenesis and bone turnover. Proc Natl Acad Sci U S A 2002;99(15):9656–9661. [PubMed: 12118119]
44. Murphy WL, Peters MC, Kohn DH, Mooney DJ. Sustained release of vascular endothelial growth factor from mineralized poly(lactide-co-glycolide) scaffolds for tissue engineering. Biomaterials 2000;21(24):2521–2527. [PubMed: 11071602]
45. Murphy WL, Simmons CA, Kaigler D, Mooney DJ. Bone regeneration via a mineral substrate and induced angiogenesis. J Dent Res 2004;83(3):204–210. [PubMed: 14981120]
46. Peng H, Usas A, Olshanski A, Ho AM, Gearhart B, Cooper GM, et al. VEGF improves, whereas sFlt1 inhibits, BMP2-induced bone formation and bone healing through modulation of angiogenesis. J Bone Miner Res 2005;20(11):2017–2027. [PubMed: 16234975]
47. Brown, CD. Ph.D. thesis. University of Washington; 2003. Cross-linked hydrogels for the delivery of growth factors in tissue engineering.
48. Hwang, JJ. Ph.D. thesis. University of Washington; 2007. Hyaluronic acid microsphere for delivery of protein therapeutics.
49. Cesaretti M, Luppi E, Maccari F, Volpi N. A 96-well assay for uronic acid carbazole reaction. Carbohydrate Polymers 2003;54(1):59–61.
50. van Dijk-Wolthuis WN, van Steenbergen MJ, Underberg WJ, Hennink WE. Degradation kinetics of methacrylated dextrans in aqueous solution. J Pharm Sci 1997;86(4):413–417. [PubMed: 9109041]
51. Zhao XB, Fraser JE, Alexander C, Lockett C, White BJ. Synthesis and characterization of a novel double crosslinked hyaluronan hydrogel. J Mater Sci Mater Med 2002;13(1):11–16. [PubMed: 15348198]
52. Wang J, Glimcher MJ, Mah J, Zhou HY, Salih E. Expression of bone microsomal casein kinase II, bone sialoprotein, and osteopontin during the repair of calvarial defects. Bone 1998;22(6):621–628. [PubMed: 9626400]
53. Nakagawa M, Kaneda T, Arakawa T, Morita S, Sato T, Yomada T, et al. Vascular endothelial growth factor (VEGF) directly enhances osteoclastic bone resorption and survival of mature osteoclasts. FEBS Lett 2000;473(2):161–164. [PubMed: 10812066]
54. Barleon B, Sozzani S, Zhou D, Weich HA, Mantovani A, Marmé D, et al. Migration of human monocytes in response to vascular endothelial growth factor (VEGF) is mediated via the VEGF receptor flt-1. Blood 1996;87(8):3336–3343. [PubMed: 8605350]

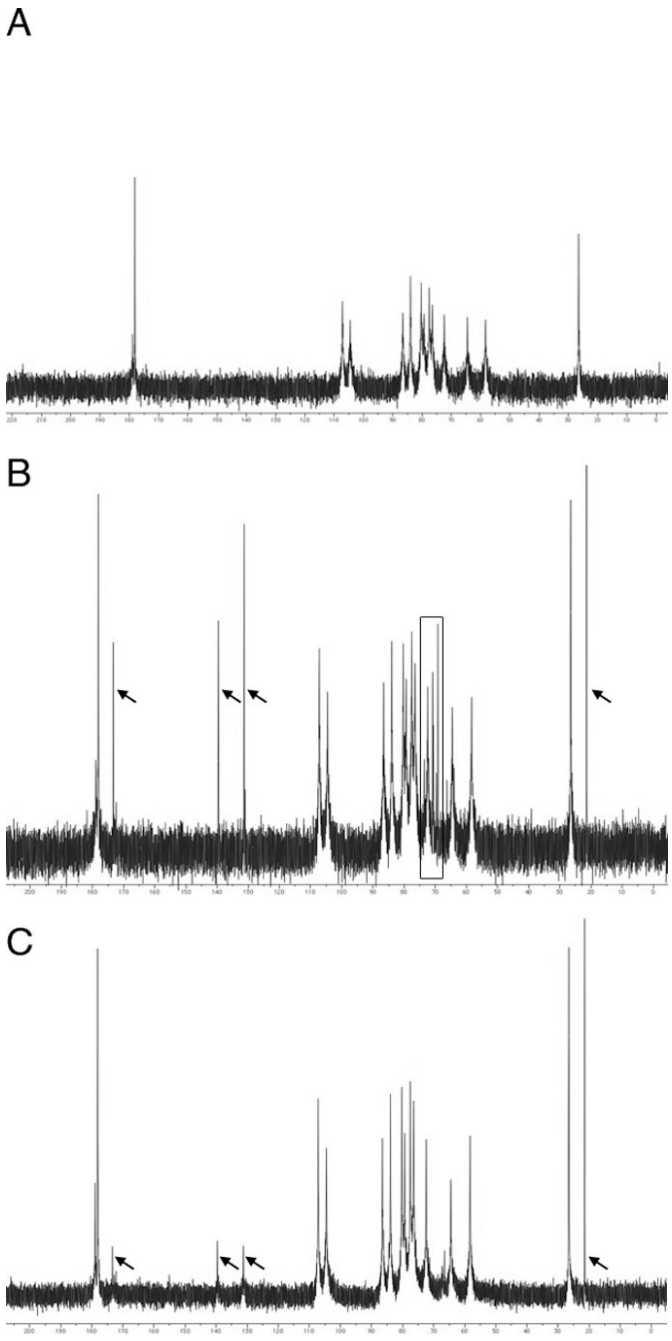

Figure 1.
^{13}C-NMR spectra. (A) Unmodified HA (220kDa). (B) HA-GMA (220kDa). (C) HA-GMA (110kDa). Arrows and box highlight additional peaks from the modification with GMA.

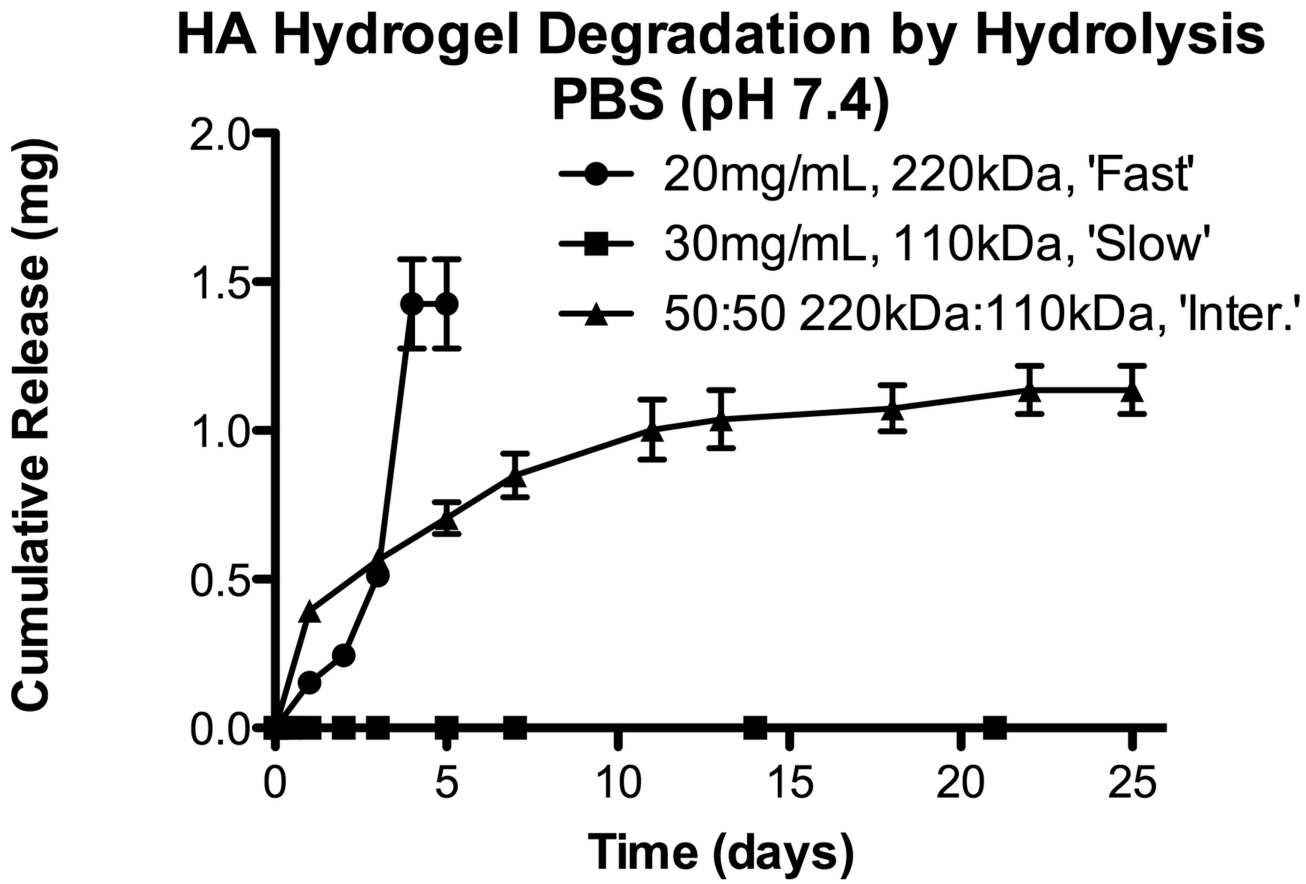

Figure 2.
Hydrolytic degradation for different HA-GMA hydrogel formulations targeting fast, intermediate, and slow degradation rates. Results are shown as mean and standard error from triplicate samples.

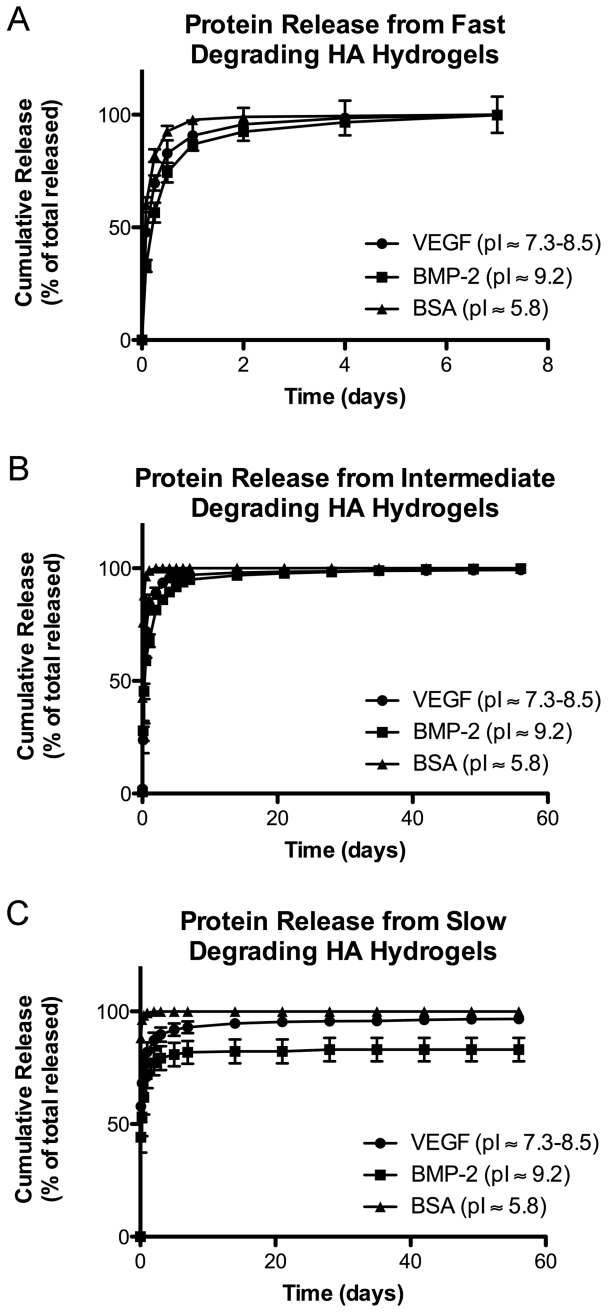

Figure 3.

Release of cationic proteins from HA-GMA hydrogels with differing degradation rates. (A) Fast (<1 week). (B) Intermediate (6–8 weeks). (C) Slow (>8 weeks). Results are shown as mean and standard error of triplicate samples.

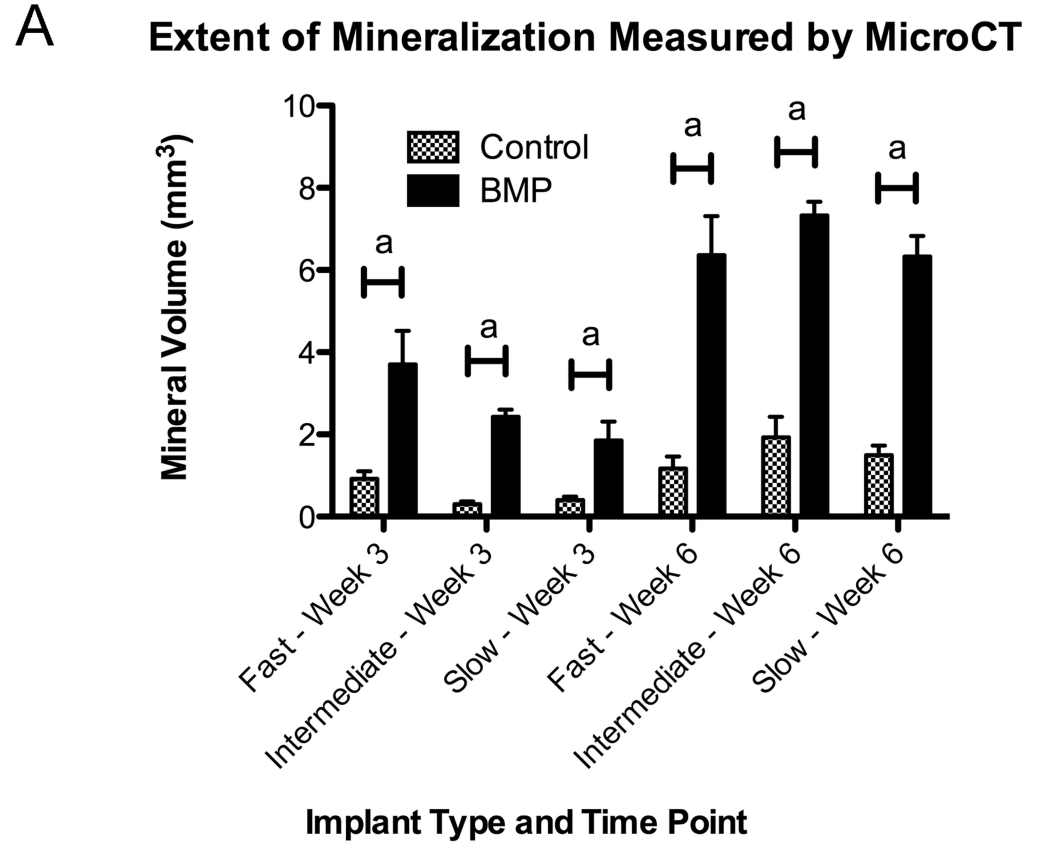

Figure 4.

(A) Extent of mineral formation induced by BMP-2 and control hydrogel scaffolds in the calvarial defect model. Results are shown as mean and standard error of a minimum n = 6. Significance at $p < 0.001^a$ was determined by three factor ANOVA followed by a Tukey HSD post-test. (B) Representative microCT images.

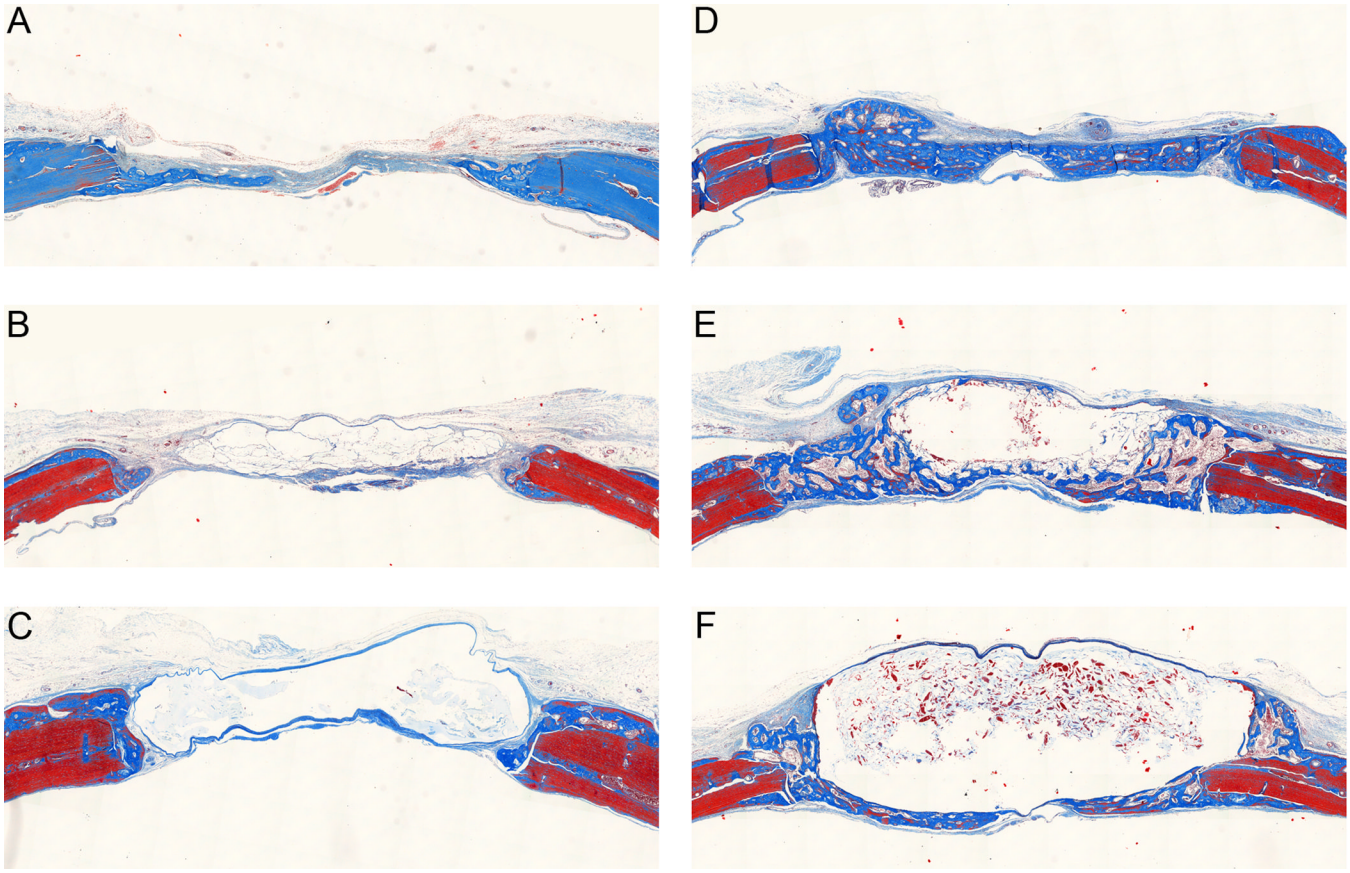

Figure 5.
Massons trichrome stained histological sections at three weeks. Representative histological sections showing cross-section of entire defect with native bone at the edges. (A) Control, fast degrading. (B) Control, intermediate degrading. (C) Control, slow degrading. (D) Fast degrading with 5μg BMP-2. (E) Intermediate degrading with 5μg BMP-2. (F) Slow degrading with 5μg BMP-2.

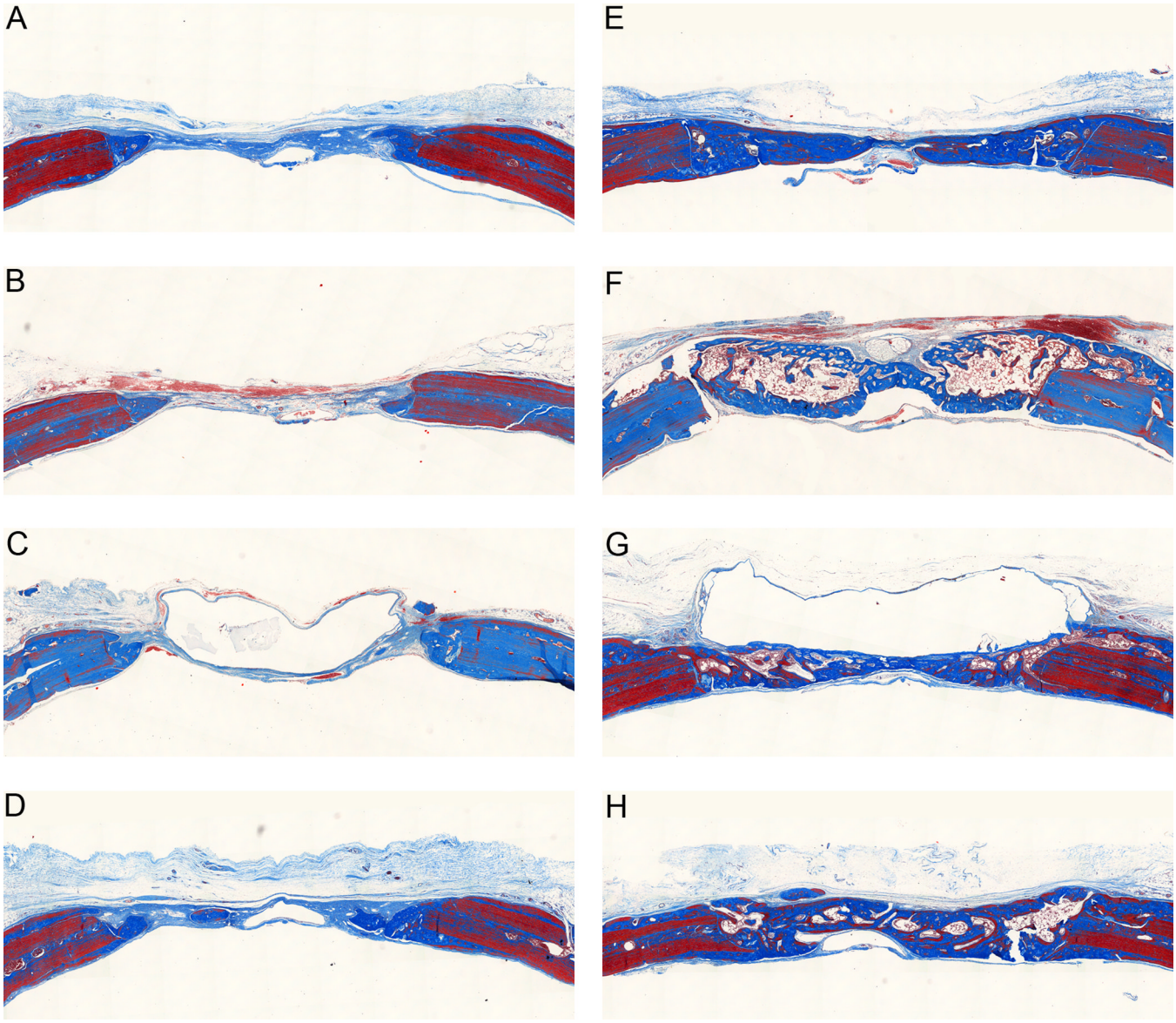

Figure 6.
Masson's trichrome stained histological sections at six weeks. Representative histological sections showing cross-section of entire defect with native bone at the edges. (A) Control, fast degrading. (B) Control, intermediate degrading. (C) Control, slow degrading. (D) Fast degrading with 25μg VEGF. (E) Fast degrading with 5μg BMP-2. (F) Intermediate degrading with 5μg BMP-2. (G) Slow degrading with 5μg BMP-2. (H) Fast degrading with 25μg VEGF and 5μg BMP-2.

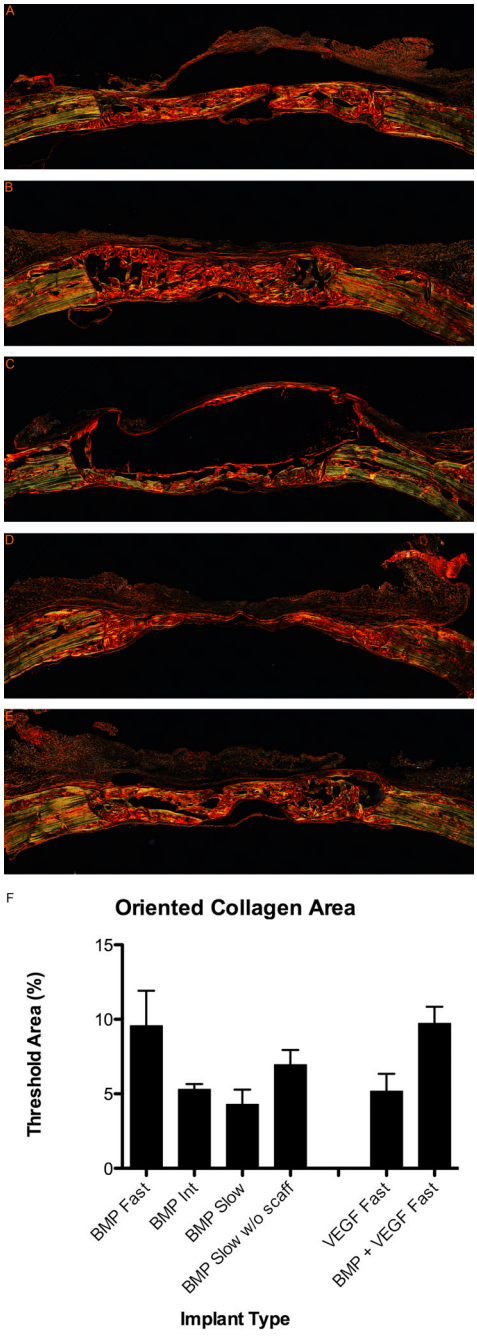

Figure 7.

Picrosirius red stain showing collagen orientation in regenerating bone at 6 weeks. Histological sections showing cross-section of entire defect with native bone at edges. (A) Fast degrading with 5μg BMP-2. (B) Intermediate degrading with 5μg BMP-2. (C) Slow degrading with 5μg BMP-2. (D) Fast degrading with 25μg VEGF. (E) Fast degrading with 25μg VEGF and 5μg BMP-2. (F) Quantification of organized bone in picrosirius red stained sections. Results are shown as mean and standard error of a minimum n = 4.

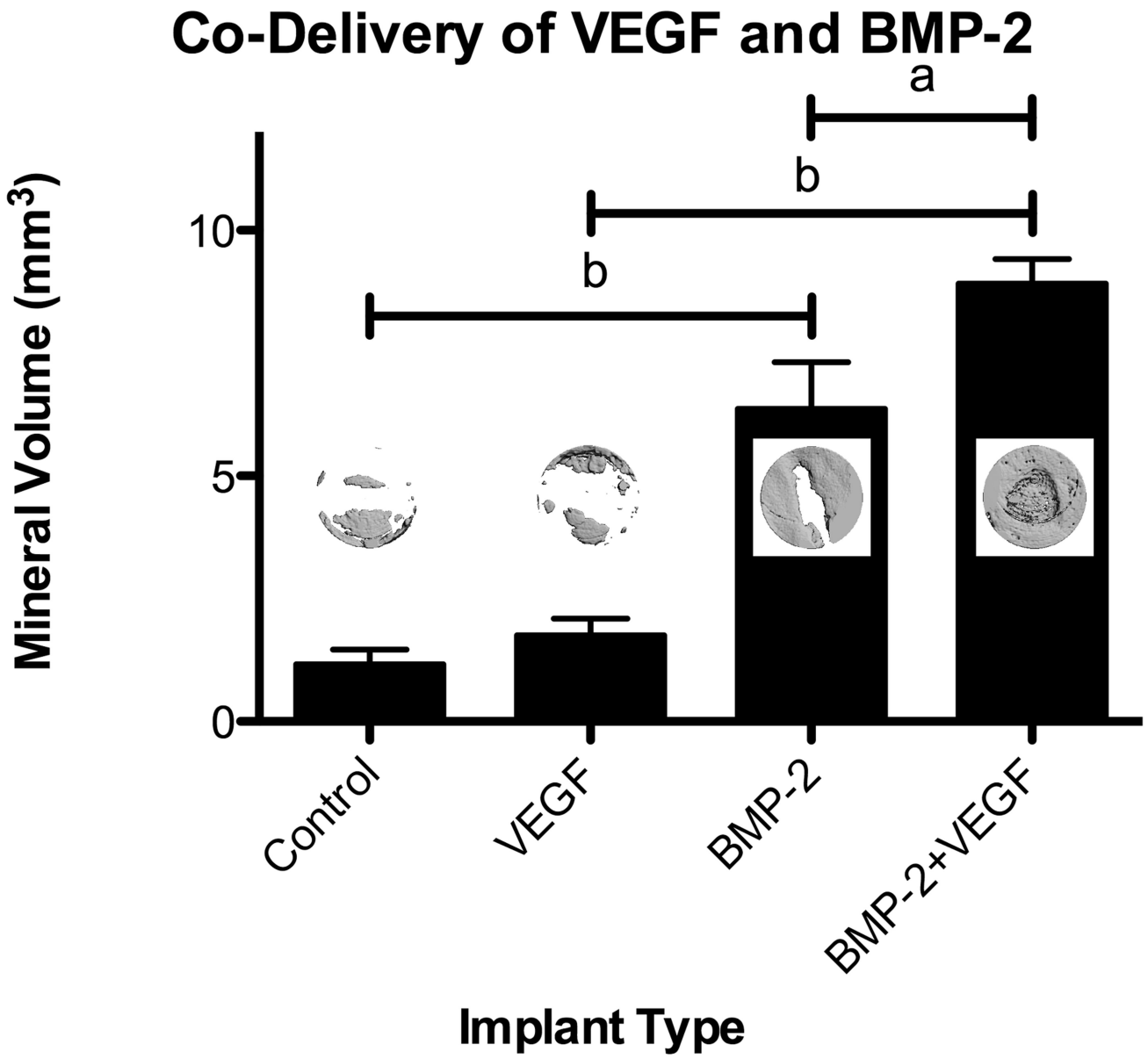

Figure 8.

Mineralization measured by microCT for co-delivery of VEGF (25μg) and BMP- 2 (5μg) from fast degrading HA hydrogels. Results are shown as mean and standard error of a minimum n = 4. Significance at $p < 0.05^a$ or $p < 0.001^b$ was determined by two factor ANOVA followed by a Bonferroni post-test. Insets show representative microCT images.